Transient Response of Soft Bonded Multilayered Shells

PHILIP UNDERWOOD*
Lockheed Palo Alto Research Laboratory, Palo Alto, Calif.
AND
C. J. BONNER,† D. W. LINDOW,† AND C. C. RANKIN‡
Lockheed Missiles & Space Company, Inc., Sunnyvale, Calif.

A computer code, based on finite difference techniques, has been developed to analyze finite length soft-bonded multilayered shells of revolution for dynamic loadings. The paper reviews the capabilities of the basic shell dynamics code used to analyze the individual shell layers and then discusses the development of the code for soft-bonded shells. The implementation of the computer code with emphasis on the bond modeling is also presented. Several numerical examples are included that provide a comparison with an analytical solution, illustrate various design parameter studies performed with the code and experimental-numerical data correlation studies. These examples serve to illustrate the validity and usefulness of the code plus the necessity of including bond deformation effects to properly analyze bonded shell structures.

I. Introduction

SHELL structures composed of two layers with a soft bond joining them are commonly used in aerospace applications; but because of the complex deformations, analyses are difficult to perform especially for dynamic environments. To aid in the design of multilayered soft bonded shell structures the TROCS (Transient Response of Coupled Shells)[1] code was developed and subsequently used in several design and experimental data correlation studies. In this paper the analysis technique for the TROCS code is presented along with several numerical studies that illustrate some of the characteristics of multi-layered soft bonded shells and numerical-experimental data correlations which clearly show the necessity of including bond deformation in the analysis.

Interest in shells with deformable bonds has been quite recent. The first investigator appears to be Payton[2] in the early 1960's. He studied bond stresses in axially loaded axisymmetric shells of semi-infinite length. Jones and Whittier[3,4] were interested in modal and dispersion characteristics of bonded shells. In related areas of study, Alzheimer et al.[5,6] analyzed cylindrical shells with cores and were mainly interested in wave propagation in the core; Ruminer and McIvor[7] recently added to this work. Longcope[8] studied the problem of a rigid cylinder within a shell-core structure. All of the above papers are essentially based on classic analytical techniques.

Numerical solutions and computer codes are also available, but they have seldom been published in the open literature. The codes available are RNGBND,[9] GIRLSIA,[10] BOND,[11] and SABOR5/DRASTIC.[12] The first three are applied to situations involving rings, and the last is for elastic shells with a shear-deformable bond. In all cases, very simple bond models are used. No computer code was available for a general inelastic finite length shell of revolution with a deformable bond that could more accurately model actual aerospace structures. This situation led to the development of the TROCS code.

Submitted April 10, 1974; presented as Paper 14-342 at the AIAA/ASME/SAE 15th Structures, Structural Dynamics, and Materials Conference, Las Vegas, Nev., April 17–19, 1974; revision received September 25, 1974. The TROCS code was developed for the U.S. Army Advanced Ballistic Missile Defense Agency, Huntsville Office, Huntsville, Ala., under Contract DAHC 60-70C-0061. The preparation of this paper was carried out under the Lockheed Missiles & Space Company's Independent Research and Development Programs.

Index category: Structural Dynamic Analysis.

* Research Scientist.

† Senior Research Engineer.

‡ Associate Research Scientist.

II. Theoretical Formulation

The TROCS code is based on the coupling of two SHORE[13,14] codes together to model the response of layered shells with a deformable bond. First a summary description of the SHORE code is given, then details of the bond coupling model and finally the computer implementation is presented.

A. SHORE Code

The equations solved by the SHORE code are those derived by Sanders[15] with provisions for linear and nonlinear kinematics, inelastic material behavior, and variable wall thickness. The formulation is restricted to shells with midsurfaces defined by a surface of revolution which eliminates many derivatives in the circumferential direction without severely restricting the class of practical problems that can be solved. The loadings considered are initial velocity, and pressure and temperature histories, all of which can be specified for each mesh point. The boundary conditions, implemented through fictitious points, include clamped, simple, and free supports plus conditions of symmetry and antisymmetry along with elastic constraints and inhomogeneous time-varying functions.

Time integration is handled with the straightforward explicit second-order central difference operator. Use of this formulation in terms of past and post displacement increments produces a solution technique most compatible with the incremental theories of plasticity. The spatial derivatives are based on two-dimensional second-order central differences in conjunction with a checkerboard (two-dimensional half-spacing) grid. Also by using the equilibrium equations in terms of stress resultants the highest derivative is limited to the second order. This technique is very accurate,[16] easily implemented due to the simple derivatives involved and very fast on the computer due to the small number of calculations required.

The plasticity formulation is based on an anisotropic yield function for both elastic perfectly-plastic and elastic-plastic linear strain hardening models (isotropic hardening). The second-order terms in the stress increments are neglected, so an algebraic solution can be obtained. In addition a fracture criterion[17] is available. Although this fracture criterion is based solely on static conditions it appears to provide satisfactory results for composite materials and sometimes doubtful results for metallics. The development of a more applicable fracture criteria for use in a structural dynamics response code is needed. To obtain the resultants, the stresses are computed at several points through the thickness, and the integrations are performed using Simpson's method. For elastic solutions, algebraic expressions are used for the integration to save computer time. In fact, throughout the

coding, algebraic forms are used wherever possible to avoid time-consuming numerical techniques.

The computational sequence of the SHORE code is as follows: starting with a new increment in time, the required boundary conditions for the displacement increments are set. The increments of strain and stress and total stress are computed, and then the check on the yield condition is made. If yielding has occurred, new stresses are computed in the plasticity subroutine. If fracture has occurred the stresses are set to zero at this point. Now, with the total stresses available, the resultants are computed, and their boundary conditions are set. Using the resultants and their derivatives in the equilibrium equations, the next increments in the three displacement quantities are computed, and the time loop commences again.

B. Bond Model

The bond is the coupling medium between the two shells as analyzed by the TROCS code. If the bond material has not failed, the motion of one shell influences the other. After a bond failure has occurred the shell motions at that point are independent unless the shells come in contact again. Based on the relative motion of the two shells at each time step plus the constitutive relationship of the bond, the influence of one shell on the other is determined. Figure 1 illustrates the over-all shell geometry plus a localized section of the wall construction that shows the bond geometry. Although the bond layer is illustrated as another shell in the model it is actually "springs" to account for normal and shear displacement stiffness. Note that for a constant Φ the u and w displacements would be together, and v would be shifted by $r(\Delta\theta/2)\sin\Phi$ due to the half spacing used in the finite difference grid. From the figure one can see that the stresses, σ_z, $\tau_{z\theta}$, $\tau_{z\Phi}$ in the bond are the surface pressures, p_z, p_θ, and p_Φ, respectively, on the inner and outer shells. The assumptions made in computing these stresses are: 1) normal and shear stresses are uncoupled in the bond; 2) normal stress is linear with strain up to a point, then cubic with strain; 3) shear stress is linear with strain; and 4) the bond is weightless. In most cases the bond weight is insignificant compared to the shell weight, but it can be included by adding extra weight to one or both shell layers.

Mathematically expressed, the relationships for the stresses are as follows:

$$\sigma_z = \frac{w_{\text{outer}} - w_{\text{inner}}}{l_b}(E_b) + (\dot{w}_{\text{outer}} - \dot{w}_{\text{inner}})(d_n) \tag{1}$$

$$\tau_{z\theta} = \left[\frac{v_{\text{inner}} - v_{\text{outer}}}{(l_b - |w_{\text{outer}} - w_{\text{inner}}|)} + \frac{\partial w_{\text{outer}}}{\partial\theta} - \frac{\partial w_{\text{inner}}}{\partial\theta}\right](G_b) + (\dot{v}_{\text{inner}} - \dot{v}_{\text{outer}})(d_s) \tag{2}$$

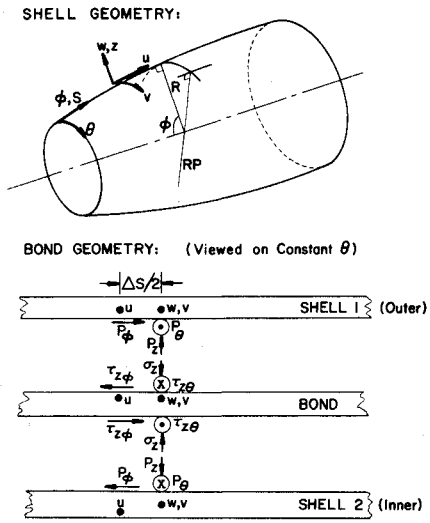

Fig. 1 Shell and bond geometry.

and $\tau_{z\Phi} = \tau_{z\theta}$ with v replaced by u, where l_b = bond thickness, E_b = bond modulus, G_b = bond shear modulus and d_n, d_s = normal, shear bond damping coefficients, respectively.

If the normal strain, the coefficient of E_b in Eq. (1), in compression exceeds ε_p then σ_z is replaced by

$$\sigma_z = \sigma_{z_1}[(1-\varepsilon_p)/(1+\varepsilon)]\,3 \tag{3}$$

where $\sigma_{z_1} = \sigma_z$ from Eq. (1) and $\varepsilon = (w_{\text{outer}} - w_{\text{inner}})/l_b$. Equation (3) provides in a physical sense for the increasing stiffness of bond materials under large compressive strains. The expression given is not based on reality, but was chosen because it provided the desired effect of keeping the two shells from occupying the same space and it works with a minimum of numerical difficulties. Of course if one knows the bond properties from experimental data, Eqs. (1–3) can be changed to fit these data and these changes are also easily made in the computer coding.

From the preceding equations it is clear that the stress in the bond is simply the strain in the bond times the appropriate modulus plus the velocity difference across the bond times the damping coefficient. The damping coefficient is computed from

$$d_{n,s} = 2\delta_{n,s}[(k_{n,s})(m_1)(m_2)/(m_1+m_2)l_b]^{1/2} \tag{4}$$

where n- normal index, s- shear index, $\delta_{n,s}$ = the assumed fraction of critical damping, $k_{n,s}$ = the bond modulus, m_1 = the mass per unit area of Shell one and m_2 = the mass per unit area of Shell two.

The selection of Δt, the integration time step, for a stable computation becomes quite complicated by the bond, as a very stiff bond can introduce a higher frequency than those present in the finite difference shell equations. For the explicit central difference operator used for the time integration in the TROCS code the time step size is limited by the magnitude of the highest frequency of the system of equations being solved.[18] When one must consider material and geometry nonlinearities plus the problem of two shells coupled together the only answer is an estimate of the highest frequency. This has been obtained by assuming one of the shells is rigid which gives the following conservative estimates (assuming the flexural frequencies are less than the extensional frequencies),

$$\Delta t \leqq \Delta s\left[\frac{1}{(g/\rho)[(E/1-v^2)+(a^2E_b/hl_b)]}\right]^{1/2} \tag{5}$$

$$\Delta t \leqq \Delta s\left[\frac{1}{(g/\rho)(E+G_b)}\right]^{1/2} \tag{6}$$

The smaller Δt must be used, where E, h, ρ = modulus, thickness, and weight density of the higher frequency shell, respectively, a = shell radius, g = gravitational constant, Δs = minimum mesh spacing, and v = Poisson's ratio. Equation (5) results from assuming radial shell motion (bond normal motion), and Eq. (6) results from assuming inplane shell motion (bond shear motion). For highly nonlinear bond moduli one must assume a bond modulus high enough to account for expected bond strains.

The TROCS code also provides for fracture of the bond in shear or normal tension; the fracture is defined through maximum allowable stresses that are input data. If a fracture occurs then no bond stresses are computed (they are set to zero) unless the shells come close enough together for a compressive strain to exist in the bond. For this condition a normal stress is computed and applied to the two shells until a tensile condition again exists in the bond.

C. Computer Implementation

The computational scheme involves the determining of the displacements in both shell layers for each time step and then computing the bond stresses which are the surface pressures for that time step. With the shell displacements known the strains and stresses can be computed, the stresses give the resultants which along with the surface pressures allow the computation of the displacements at the end of the time step and the process continues up to the time requested. To produce this sequence of events on the computer mainly involves bookkeeping

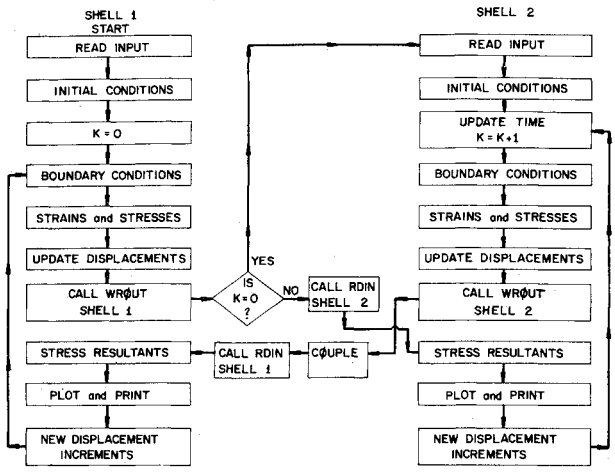

Fig. 2 TROCS code flowchart.

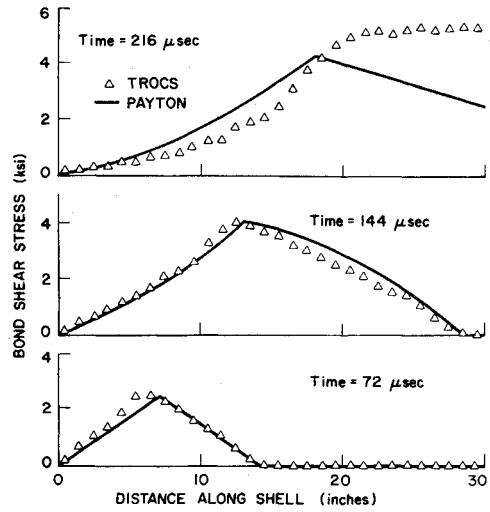

Fig. 3 TROCS comparison with Payton's analytical solution.

procedures to keep the data for the two shells separate; this is done as follows.

In addition to the instructions for the SHORE code which solves the shell dynamics problem three additional subroutines are used to produce the TROCS code. The first, called COUPLE, performs the calculations of the bond stresses as discussed in Sec. II-B. The other two, called WROUT and RDIN, are NTRAN (UNIVAC-oriented computer operation) based routines that write on a disk and read from a disk. In the WROUT routine, all the quantities needed for the computation of the shell dynamics problem at the next time step are written onto the disk. In the RDIN routine, the same quantities are read into the core from the disk; thus, two disk units of sufficient size are set up to store the data for Shell 1 (outer layer) and Shell 2 (inner layer). While the code is computing the response of one shell, the data for the other shell are stored on the disk.

By going through the flowchart for the TROCS code, shown in Fig. 2, the procedure becomes more clear. From the starting point, on the first time step $k = 0$, the input data for Shell 1 are read in; next, the initial conditions, boundary conditions, strains and stresses, and the updated displacements are computed. At this point the data for Shell 1 are written onto the disk. The bond input data and input data for Shell 2 are read in next. The same computations made for Shell 1 are now performed on Shell 2 except now the time index k is updated. The displacements, velocities, etc., are now known at the end of the first time step for both shell layers, so the COUPLE routine is called to compute the bond stresses (the surface pressures on the shells). The data for Shell 1 are read into the core from the disk, and the new displacements are computed. Then, the data read onto the disk, and the data for Shell 2 are read into the core. The new displacements are computed for Shell 2; again the shell displacements, etc. are known at the same point in time and the COUPLE routine is called. After $k > 0$, the computational sequence is not altered.

The response data for the two shell layers and the bond are printed at selected time intervals; unwanted quantities may be suppressed, and time history plots of the response data may be obtained for any mesh point on either shell. Since the TROCS code actual computes the response for two shells plus the coupling calculations the computer run times are approximately 2.1 times greater than a computer run for an equivalent shell with the SHORE code.

III. Numerical Studies

In this section, several numerical examples are presented relating to code checkout, design parameter studies, and experimental-numerical correlation studies. These examples serve to illustrate the validity of TROCS and application of the code to design problems. To provide a check with an analytical solution a problem solved by Payton,[2] the determination of the bond stress in the coupling of two dissimilar semi-infinite axisymmetric shells subjected to a step end velocity, was solved numerically with the TROCS code for a simply supported finite length shell. Since the numerical solution is for a finite length shell the comparison will only be valid up to the time of wave reflection from the unloaded boundary of the shell. The results of this comparison are shown in Fig. 3 for an axisymmetric step end velocity of 707 in./sec and the following shell properties; outer shell layer; length = 30.0 in., $\Delta s = 1.0$ in., density = 0.25 lb/in.^{3}, Poisson's ratio = 0, modulus = 5×10^6 psi, radius = 1000 in. and thickness = 1.0 in.; inner shell layer; length = 30 in., $\Delta s = 1.0$ in., density = 0.1 lb/in.^{3}, Poisson's ratio = 0, modulus = 10×10^6 psi, radius = 998.9 in. and thickness = 1.0 in.; bond; $E_b = 10{,}000$ psi and $G_b = 5000$ psi, undamped. Due to the difference in sound speeds for the inner (0.1965 in./μsec) and outer (0.0878 in./μsec) shell layer the disturbance from the step end velocity propagates faster in the

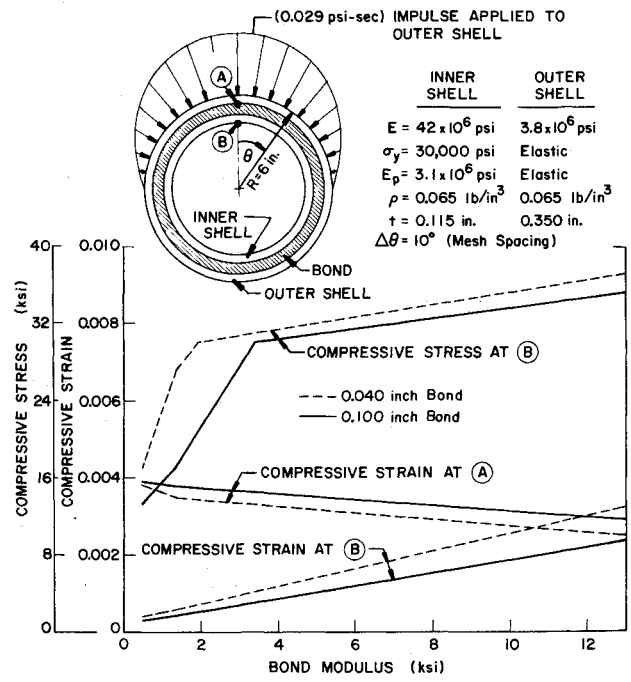

Fig. 4 Bond modulus and thickness study.

Table 1 Bond stresses for varying initial debonding and impulse partitioning

	±10° Debonded				±20° Debonded			
	50/50[a]		0/100[b]		50/50[a]		0/100[b]	
θ	Normal psi	Shear psi	Normal psi	Shear psi	Normal psi	Shear psi	Normal psi	Shear psi
0°	...	...	...	...	...	...	...	...
30°	−670/+70	−30/+60	−725/+60	−30/+110	−700/+50	−40/+70	−800/+70	−55/+140
60°	−450/+80	−37/+70	−480/+80	−30/+87	−490/+80	−45/+75	−540/+65	−40/+105
90°	−380/+100	−35/+75	−400/+100	−20/+80	−400/+100	−40/+75	−440/+100	−30/+87
120°	−320/+100	−30/+65	−340/+100	−20/+68	−340/+100	−30/+65	−370/+100	−17/+70
180°	−400/+90	−8/+3	−465/+100	−8/+3	−460/+100	−7/+3	−500/+120	−8/+2

	±40° Debonded				±65° Debonded			
	50/50[a]		0/100[b]		50/50[a]		0/100[b]	
θ	Normal psi	Normal Shear psi	Shear Normal psi	Normal Shear psi	Shear Normal psi	Normal Shear psi	Shear Normal psi	Shear psi
0°	...	...	...	...	...	...	...	...
30°	...	...	...	...	...	...	...	...
60°	−560/+70	−50/+85	−650/+100	−45/+14	...	...	...	...
90°	−440/+80	−40/+80	−500/+90	−24/+105	−470/+80	−37/+80	−540/+65	−20/+125
120°	−360/+100	−30/+70	−410/+110	−17/+75	−390/+80	−27/+70	−440/+110	−15/+80
180°	−500/+120	−8/+2	−570/+150	−9/+2	−520/+110	−3/+3	−600/+180	−10/+2

[a] Impulse Partitioning 50/50: Where bond has failed 50% of the impulse imparted to the outer shell, 50% to the inner shell, where no bond failure shells have equal velocities.
[b] Impulse Partitioning 0/100: Where bond has failed all of the impulse is imparted to the inner shell, where no bond failure shells have equal velocities.

inner layer than the outer layer, producing a relative axial displacement between the shell layers that results in the bond stress. Indeed in the results one sees the bond stress is a maximum just before the arrival of the wave front in the outer shell as this is obviously the point of maximum relative displacement between the two shell layers. From Fig. 3 it is seen that the numerical calculations are in good agreement with the analytical solution for the bottom two sketches which illustrate times before reflection. The upper sketch illustrates a time after reflection occurs in the TROCS calculations, so agreement is not expected.

As a design exercise to study the effects of bond modulus and thickness, the ring configuration sketched in Fig. 4 was analyzed for a cosine distribution of impulse over half the circumference. The peak compressive strains and stresses computed at $\theta = 0°$ are shown in Fig. 4 for 40 mil and 100 mil bond thicknesses vs the bond modulus (normal direction). The bond shear modulus was chosen to be the bond modulus divided by 2.9. The softer bond produces a better protection of the inner

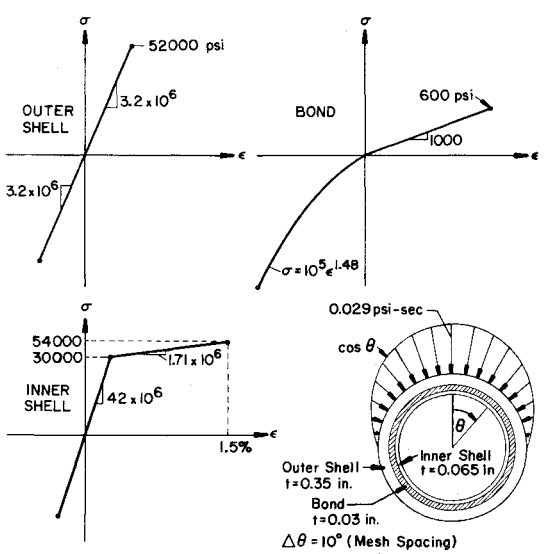

Fig. 5 Ring geometry and material properties for the results shown in Tables 1 and 2.

shell as would be expected. For a larger magnitude loading a soft bond may lead to troubles unless it is thick enough to prevent the bond from "bottoming out". Or one can select a bond modulus that would provide an efficient structure in which both rings would carry ultimate strains or stresses. As one would expect a thicker bond produces a softening effect. To prevent yield of the inner ring the stress would have to keep below 30 ksi which, from the curve for the stresses, requires a very soft bond, i.e. a modulus of 2–3 ksi.

In another design study a 12 in. o.d. two-layered ring coupled together with a deformable bond was analyzed to determine bond stresses and strains and deformations of the inner shell due to the effects of varying degrees of initial debonding and impulse partitioning. The basic material properties and ring geometry are sketched in Fig. 5; in addition the bond shear modulus = 345 psi and damping coefficients d_n, $d_s = 0.169, 0.099$ lb-sec/in.^{3}, respectively were chosen. The densities are 0.065 lb/in.^{3} for both shells. The impulse was distributed as a cosine over half the circumference with a peak value of 0.029 psi-sec as in the previous example. Presented in Table 1 are the maximum compressive and tensile bond stresses for the normal and shear components for various locations around the circumference vs degrees of initial debonding and impulse partitioning. Examination of Table 1 indicates that the range of bond stresses varies more with the 0/100 impulse partitioning than they do with the 50/50 partitioning. In all cases the debonding will not propagate beyond the initial value, assuming a normal tensile failure stress of 600 psi for the bond. Shown in Table 2 are the maximum compressive inner fiber circumferential strain and the maximum radial displacement for the inner ring vs degrees of debonding and impulse partitioning. Table 2 shows that the maximum strain at 0° increases much more rapidly for the various degrees of debonding for 0/100 impulse partitioning than for the 50/50 case. The maximum radial displacement at 0° does not show a significant change due to debonding, however the magnitude doubles as the impulse partitioning changes with the 0/100 case being the most severe.

A similar study for a finite length (12 in.) conical frustrum was also performed. The material properties shown in Fig. 5 still apply, but the data for the inner shell now represents the effective stress-strain curve. The outer shell is 0.30 in. thick and has an outside radius (normal to the shell wall) of 5.975 in. at the small end and 7.545 in. at the large end. The inner shell is 0.055 in. thick and the densities, bond damping, and

Table 2 Maximum inner fiber circumferential strain and radial displacements for various degrees of debonding and impulse partitioning

	±10° Debonded				±20° Debonded			
	50/50[a]		0/100[b]		50/50[a]		0/100[b]	
θ	ε_{max}	W_{max}	ε_{max}	W_{max}	ε_{max}	W_{max}	ε_{max}	W_{max}
0°	−0.097%	−0.028	−0.31%	−0.053	−0.18%	−0.026	−0.51%	−0.051
30°	−0.095%	−0.0175	−0.175%	−0.0155	−0.155%	−0.0175	−0.42%	−0.016
60°	−0.07%	−0.005	−0.075%	−0.0085	−0.07%	−0.0047	−0.092%	−0.0086
90°	−0.067%	+0.0118	−0.07%	+0.0113	−0.07%	+0.011	−0.07%	+0.0086
120°	−0.057%	+0.0118	−0.06%	+0.0110	−0.057%	+0.011	−0.063%	+0.10
180°	−0.08%	+0.0062	−0.085%	+0.0057	−0.088%	+0.006	−0.093%	+0.005
	±40° Debonded				±65° Debonded			
	50/50[a]		0/100[b]		50/50[a]		0/100[b]	
θ	ε_{max}	W_{max}	ε_{max}	W_{max}	ε_{max}	W_{max}	ε_{max}	W_{max}
0°	−0.27%	−0.027	−0.7%	−0.049	−0.27%	−0.027	−0.72%	−0.054
30°	−0.13%	−0.026	−0.42%	−0.041	−0.18%	−0.023	−0.54%	−0.040
60°	−0.072%	−0.0045	−0.135%	−0.008	−0.06%	−0.0127	−0.155%	−0.021
90°	−0.07%	+0.010	−0.08%	+0.0082	−0.07%	+0.0105	−0.097%	+0.0087
120°	−0.057%	+0.011	−0.07%	+0.010	−0.057%	+0.0105	−0.075%	+0.0088
180°	−0.10%	+0.006	−0.11%	+0.0045	−0.092%	+0.006	−0.115%	+0.0048

[a] Impulse Partitioning 50/50: Where bond has failed 50% of the impulse imparted to the outer shell, 50% to the inner shell, where no bond failure shells have equal velocities.
[b] Impulse Partitioning 0/100: Where bond has failed all of the impulse is imparted to the inner shell, where no bond failure shells have equal velocities.

bond shear modulus are the same as the previous example. Poisson's ratio is 0.2 for the outer shell and 0.06 for the inner shell. The bond thickness is 0.030 in. The total impulse is 0.029 psi-sec applied in the cosine distribution over half the circumference and uniform along the length. The cone is clamped at the small end and clamped without a rotation restriction at the large end. Response data for the case of initial debonding over $\pm 90°$ of the shell at a point located at $\theta = 0°$ (under the peak loading) and at $S = L/2$ (the midpoint) for varying impulse partitioning is shown in Fig. 6. The results follow the same trend as the ring results presented in Table 2. Also, note the meridional strain peaks follow the same trend as the circumferential strain, but at a lower magnitude. For the particular example the ring and shell results provide similar guides for a design, but for a case with considerable deformation and/or fracturing of the shell material the results for the ring and shell would not be comparable.

Two examples from experimental-analytical correlation studies are described below. The first is for a ring with properties and loading similar to the two previously studied ring designs. The ring has a 9.0 in. o.d. and the outer layer is impulsively loaded with a cosine distribution over half the circumference with a peak of 0.0338 psi-sec. The outer ring layer has the following properties: density = 0.049 lb/in.^{3}, thickness = 0.41 in., $E = 1.59 \times 10^6$ psi, tensile yield = 10.4 ksi, compressive yield = 33.6 ksi, tensile plastic modulus = 1.72×10^5 psi and compressive plastic modulus = 6.7×10^5 psi. The bond properties are: thickness = 0.03 in., shear modulus = 80 psi, normal modulus = 1.8×10^4 psi for strains less than 50,000 $\mu\varepsilon$ and 4.77×10^4 for strains greater than 50,000 $\mu\varepsilon$, and 5% damping is included. The inner ring layer has the following properties: density = 0.066 lb/in.^{3}, thickness = 0.065 in., $E = 41.8 \times 10^6$ psi, yield = 46 ksi, and the plastic modulus = 8.9×10^5 psi. The numerical calculations were made with the TROCS code which includes the bond deformations and the SHORE code which assumes a rigid bond. Figure 7 illustrates the inner surface circumferential strain for the inner ring at 0°, 60°, and 180° (0° under the peak load) as computed by SHORE and TROCS and compared with experimental data.[19] At all locations it is easily seen that the computations based on a deformable bond (TROCS) are superior to the rigid bond or Kirchhoff assumption (SHORE) based calculations. Indeed without the deformable bond calculations there would not be any correlation. The loading for the experiment was not very severe and the data correlation is quite good and typical of low level tests.

At the other extreme the TROCS code was used in a correlation study for a 24 in. o.d. cylinder (21 in. long with simulated simple support boundaries) subjected to an asymmetric blast loading.[20] In this particular test the bond failed over the entire shell due to large deformations and the brittle outer shell was completely removed. This was substantially predicted by the code calculations. The times at which the fractures occur and where they start are difficult to determine unless one obtains a huge amount of code output. From the limited output of stresses for

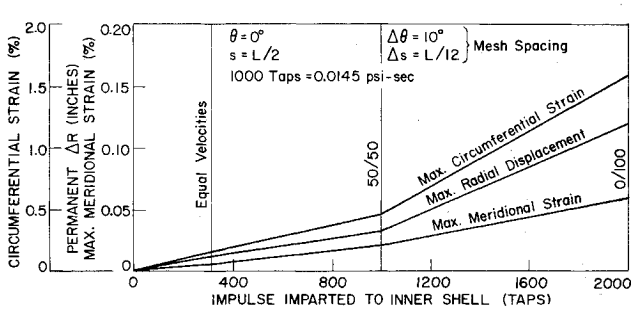

Fig. 6 Conical shell frustum study for initial debonding and impulse partitioning.

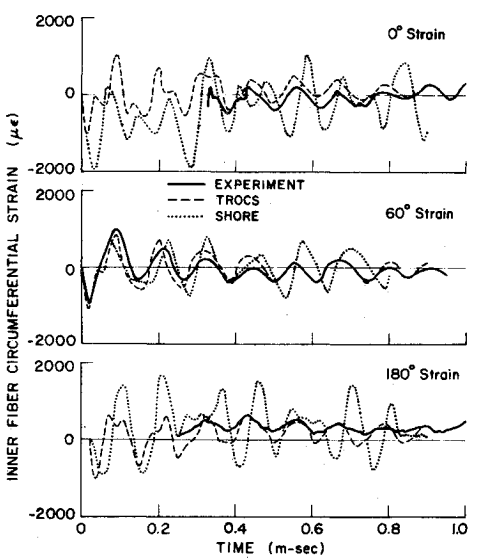

Fig. 7 Comparison of SHORE and TROCS computations with experimental ring data.

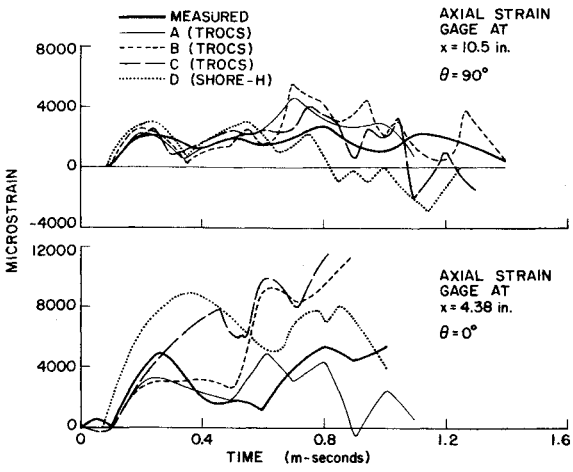

Fig. 8 Comparison of SHORE and TROCS computations with experimental cylindrical shell data.

this study the fractures appear to start under the peak load near the boundaries and spread throughout the shell. In this case first fracture occurred very early in time and was completed at approximately 1 ms.

This particular example was used to study predicted response for various material property models that are shown in Table 3. In addition the basic properties are: for the outer shell layer, $E = 2.94 \times 10^6$ psi up to 20 ksi and then $E = 2.74 \times 10^5$ psi (bi-linear elastic), thickness = 0.5 in., density = 0.052 lb/in.^{3} and Poisson's ratio = 0.25; for the bond, normal modulus = 40 ksi, shear modulus = 13 ksi, thickness = 0.060 in.; for the inner shell layer $E = 10 \times 10^6$, E_p (plastic modulus) $= 8.3 \times 10^4$ psi, thickness = 0.2 in., density = 0.1 lb/in.^{3} and Poisson's ratio = 0.25. The pressure loading was uniform along the length of the shell and distributed circumferentially as:

$$P = P_o \cos\theta e^{-t/\tau} \qquad 0 \leqq \theta \leqq 80°$$
$$P = P_o \cos(80°) e^{-t/\tau} \qquad \theta \geqq 80°$$

where $P_o = 2130$ psi and $\tau = 0.82$ msec. The pressure loading wave front wave engulfed the shell at a velocity of 4930 fps. The shell was modeled with planes of symmetry at $S = L/2$ and $\theta = 0°, 180°$. The spacing used was $\Delta s = 0.875$ in. and $\Delta\theta = 10°$. The boundary conditions were classical simple supports except $N_\Phi = 0$ instead of the usual $u = 0$.

Strain gages were mounted on the inner surface of the inner shell and selected correlations with the TROCS and SHORE code are shown in Fig. 8. The *A, B, C*'s refer to the various material property models used for the TROCS analysis and *D* pertains to the SHORE code analysis; these properties are shown in Table 3. Although the correlations are not as good as for the previous low level test, the calculations are certainly indicative of the strain levels recorded during the test. The material Model *A* but with Model *B* bond properties was chosen for future correlation work. Again the SHORE code which does not include a deformable bond does not produce as good a correlation as the TROCS code for this experiment, especially if one considers the TROCS code prediction of complete bond fracture and outer shell layer removal.

Of course an excellent correlation was not obtained for this test, but an engineer is quite pleased to come this close considering the severe environment of this test. That is the measurements are difficult to obtain, the material properties are vague and the deformations so large that the validity of shell equations used becomes doubtful; yet the analysis provides a very good bound on the experimental data. This correlation is even more remarkable when one considers that for the simpler problem, only nonlinear geometry and a single wall shell, it is difficult just to get independently developed codes to agree.[21] Other tests in this series[20] had contact gages for measuring the shell displacement at the midpoint under the peak load. A displacement of 2 in. was recorded at 1.38 msec for one test and at 0.83 msec for another test; the computed time values from the TROCS code were 1.15 msec and 0.74 msec, respectively. It is easy to see that if one only had to provide predicted displacements life would be much simpler.

Table 3 Materials property data for cylinder correlation study

Case	Inner shell			Outer shell	Bond
	Yield	Fracture	Plasticity	Fracture	Fracture
A	$\sigma_y = 47$ ksi	72 ksi C[a]	Linear	28 ksi T	3800 psi T
		65 ksi T[a]	Strain	31 ksi C	
	$\tau_y = 27$ ksi	36 ksi S[a]	Hardening		2300 psi S
B	$\sigma_y = 47$ ksi	100 ksi C	Linear	28 ksi T	1000 psi T
		100 ksi T	Strain	31 ksi C	
	$\tau_y = 27$ ksi	100 ksi S	Hardening		600 psi S
C	$\sigma_y = 35$ ksi	None	Perfectly	28 ksi T	1000 psi T
	$\tau_y = 20$ ksi	None	Plastic	45 ksi C	600 psi T
D	Same as B, except no bond properties				

[a] C Compression, T Tension, S Shear.

Conclusions

The development of a relatively sophisticated two-dimensional shell dynamics code for studying multilayered shells with a deformable bond has been presented. Though better numerical techniques and modeling techniques still need to be pursued, as in any of the sophisticated structural analysis codes available today. The bond model, for example, was derived mostly by default, due to the lack of material behavior data. It is felt that the TROCS code is a unique analysis tool for shells of revolution under asymmetric dynamic loading including the effects of nonlinear material behavior and geometry with a deformable bond. The usefulness of the code has been demonstrated through the design parameter studies and its validity and necessity has been illustrated by correlations between numerical and experimental results.

References

[1] Underwood, P. G., "TROCS (Transient Response of Coupled Shells) User's Manual," LMSC-D266238, March 1972, Lockheed Missiles & Space Co., Sunnyvale, Calif.

[2] Payton, R. G., "Bond Stress in Cylindrical Shells Subjected to an End Velocity Step," *Journal of Mathematics and Physics*, Vol. XLIII, No. 3, 1964, p. 169.

[3] Jones, J. P. and Whittier, J. S., "Axially Symmetric Motion of a Two-Layered Timoshenko Type Cylindrical Shell," *Journal of Applied Mechanics*, Vol. 33, No. 4, March 1966, pp. 838–844.

[4] Whittier, J. S. and Jones, J. P., "Axially Symmetric Wave Propagation in a Two-Layered Cylinder," *International Journal of Solids and Structures*, Vol. 3, July 1967, pp. 657–675.

[5] Alzheimer, W. E., Forrestal, M. J., and Murfin, W. B., "Transient Response of Cylindrical Shell-Core System," *AIAA Journal*, Vol. 6, No. 10, Oct. 1968, pp. 1861–1866.

[6] Forrestal, M. J., Alzheimer, W. E., and Longcope, D. B., "Transient Response of a Cylindrical Shell Containing an Orthotropic Core," *AIAA Journal*, Vol. 8, No. 9, Sept. 1970, pp. 1638–1643.

[7] Ruminer, J. J. and McIvor, I. K., "Dynamic Response of an Elastic Cylindrical Shell-Solid Core Composite Subject to Time-Dependent Loading," *AIAA Journal*, Vol. 9, No. 10, Oct. 1971, pp. 1991–1996.

[8] Longcope, D. B., "Motion of a Rigid Cylinder Within a Shell-Core Structure," *AIAA Journal*, Vol. 8, No. 5, May 1970, pp. 967–968.

[9] Franke, R., "RINGBOND, A Computer Program for Multiple Layered Rings," Kaman Nuclear, KN-68-397, Nov. 1965, Kaman Aerospace Corp., Bloomfield, Conn.

[10] Massard, J. M., "GIRLS I AND IA—General Inelastic Response of Layered Shells," LMSC L-41-66-12, Sept. 1966, Lockheed Missiles & Space Co., Sunnyvale, Calif.

[11] Chane, H. L., "Dynamic Elastic-Plastic Response of Soft Bonded Rings," DAC 63079, Jan. 1969, McDonnell Douglas Astronautics Company/Western Division, Huntington Beach, Calif.

[12] Cwiertny, A. J., Jr., "SABOR5/DRASTIC V User's Manual," SAMSO TR70-110, Feb. 1970, Air Force Space and Missile Systems Organization.

[13] Underwood, P. G., "User's Guide to the SHORE Code," LMSC-D244589, Jan. 1973, Lockheed Missiles & Space Co., Sunnyvale, Calif.

[14] Underwood, P., "Transient Response of Inelastic Shells of Revolution," *Computers & Structures*, Vol. 2, Dec. 1972, pp. 975–989.

[15] Sanders, J. L., Jr., "Nonlinear Theories for Thin Shells," *Quarterly of Applied Mathematics*, Vol. XXI, No. 1, Jan. 1963, pp. 21–36.

[16] Underwood, P., "Accuracy of Finite Difference Representations for the Transient Response Analysis of Shells," *Earthquake Engineering and Structural Dynamics*, Vol. 2, 1974, pp. 219–233.

[17] Hoffman, O., "The Brittle Strength of Orthotropic Materials," *Journal of Composite Materials*, Vol. 1, No. 2, April 1967, pp. 200–206.

[18] Leech, J. W., Hsu, P. T., and Mack, E. W., "Stability of a Finite Difference Method for Solving Matrix Equations," *AIAA Journal*, Vol. 3, No. 11, Nov. 1965, pp. 2172–2173.

[19] Wieselmann, P., private communication, Kaman Sciences Corp., Colorado Springs, Colo., Sept. 1973.

[20] Bonner, C. J., Internal LMSC Rept., Sept. 1973, Lockheed Missiles & Space Co., Sunnyvale, Calif.

[21] Ball, R. E., Hubka, W. F., and Huffington, N. J., Jr., Underwood, P., and Von Riesemann, W. A., "A Comparison of Computer Results for the Dynamic Response of the LMSC Truncated Cone," *Computers & Structures*, Vol. 4, May 1974, pp. 485–498.